MIT Libraries | DSpace@MIT

MIT Open Access Articles

Multilayer Graphene—A Promising Electrode Material in Liquid Cell Electrochemistry

The MIT Faculty has made this article openly available. ***Please share*** how this access benefits you. Your story matters.

Citation: Tan, S. F., Reidy, K., Lee, S., Klein, J., Schneider, N. M., Lee, H. Y., Ross, F. M., Multilayer Graphene—A Promising Electrode Material in Liquid Cell Electrochemistry. Adv. Funct. Mater. 2021, 31, 2104628.

As Published: http://dx.doi.org/10.1002/adfm.202104628

Publisher: Wiley

Persistent URL: https://hdl.handle.net/1721.1/140408

Version: Author's final manuscript: final author's manuscript post peer review, without publisher's formatting or copy editing

Terms of use: Creative Commons Attribution-Noncommercial-Share Alike

Massachusetts Institute of Technology

Check for updates

Author Manuscript

Multilayer Graphene – A Promising Electrode Material in Liquid Cell Electrochemistry

*Shu Fen Tan, Kate Reidy, Serin Lee, Julian Klein, Nicholas M. Schneider, HaeYeon Lee and Frances M. Ross**

Dr. S. F. Tan, Ms. K. Reidy, Ms. S. Lee, Dr. J. Klein, Dr. H.Y. Lee, Prof. F. M. Ross

Department of Materials Science and Engineering, Massachusetts Institute of Technology, Cambridge MA 02139, United States

E-mail: fmross@mit.edu

Dr. N. M. Schneider

Renata Global, Cambridge MA 02139, United States

Keywords: Liquid cell, Graphene electrode, In situ TEM, Electrochemistry

Abstract: The combination of imaging with electrochemical quantification in liquid cell transmission electron microscopy (TEM) provides opportunities for visualizing material processes in liquid with good spatial and temporal resolution in a way that is inaccessible in bench-top electrochemical experiments. The electrode material used in liquid cell TEM determines the reliability and consistency of the electrochemical measurements, and also influences the resolution when imaging processes on the electrode. Here, we explore the opportunities arising from the use of 2D materials in liquid cell electrochemistry. Through electrochemical imaging and modelling we demonstrate that the use of graphene electrodes enables quantitative electrochemical metal deposition studies and we suggest that the minimal electron scattering and electric-field enhanced wettability are advantageous in obtaining interpretable and higher resolution data. We anticipate that incorporation of 2D materials into electrode design will open new opportunities for investigating problems in crystal growth, energy storage and electrocatalysis.

This is the author manuscript accepted for publication and has undergone full peer review but has not been through the copyediting, typesetting, pagination and proofreading process, which may lead to differences between this version and the Version of Record. Please cite this article as doi: 10.1002/adfm.202104628.

This article is protected by copyright. All rights reserved.

Author Manuscript

1. Introduction

Electrochemical processes are central to energy storage applications ranging from batteries and fuel cells to electrolyzers that allow the storage of chemical energy in matter and its conversion into electricity. Recent advances in microelectromechanical system (MEMS)[1] manufacturing technology enable the miniaturization of conventional electrochemical setups into compact vacuum-sealed units – liquid cells that can be fitted into the column of the electron microscope. This has enabled liquid cell transmission electron microscopy (TEM) to emerge as a powerful electrochemical characterization technique that allows real-time imaging of electrochemical processes at high spatial and temporal resolution.[2-4] Electrochemical liquid cell TEM has been used to study a wide range of problems pertaining to electrochemical deposition[4-7] as well as energy storage and electrocatalysis, including understanding solid-electrolyte interface formation,[8] lithiation in anode and cathode materials[9] and electrochemical growth or etching behaviour of solid electrocatalysts.[10, 11]

The choice of electrode materials in liquid cell TEM is critical for several distinct reasons. The electrodes must allow the process that takes place within the liquid cell to replicate the "real life" process as closely as possible. They must ensure consistent and reliable electrochemical measurements. But it is also important that the electrode material does not scatter electrons strongly. The resolution in liquid cell TEM is often dose-limited due to the sensitivity of the electrolyte to electron beam irradiation.[12, 13, 14] The signal to noise ratio, which controls resolution under dose-limited circumstances, depends on the mass thickness of all the components in the electrochemical cell. This includes the windows and liquid layer, and also the electrode, particularly when observing phenomena that take place over the surface of the electrode (as opposed to around the edges). Pt[2, 15] and Au[4, 5] are the most commonly used electrode materials in state-of-the-art electrochemical MEMS thin window cells. Pt and Au are undoubtedly beneficial due to their stability

This article is protected by copyright. All rights reserved.

Author Manuscript

to corrosion and their high conductivity, even as thin films. Nonetheless, they contribute a large mass contrast and a non-uniform background due to their polycrystalline nature. Moreover, Pt is also known to be sensitive towards changes in electrolyte composition, such that the presence of oxygen and hydrogen or pH change can result in dissolution.[16] The adhesion layer, commonly Cr or Ti, that is required for fabricating these metal electrodes can further increase the complexity of the electrochemical system. Recent *in situ* electrochemical studies with the use of glassy carbon electrodes[11, 15, 17, 18] show improved image quality but the material is relatively difficult to pattern and prone to mechanical damage, despite its good cathodic potential range.[19] Another major issue faced by the carbon electrode is wetting: the carbon film is hydrophobic and often requires surface modification to improve its hydrophilicity[20] which further complicates electrochemical measurement and data interpretation. Indium tin oxide (ITO) has low sheet resistance and high transmittance.[21] It is a promising transparent material for liquid cell TEM electrodes but it is hindered by its poor mechanical stability and compatibility with acidic solutions.[22]

Two-dimensional (2D) materials such as graphene and transition metal dichalcogenides (TMDs) are potential candidate materials for electrodes due to their exceptional intrinsic properties, particularly high surface-to-volume ratio, electrical charge mobility, thermal conductivity and mechanical strength.[23, 24] Graphene in particular shows tuneable band structure and electrocatalytic activity, excellent conductivity, good chemical resistance and mechanical flexibility and is widely used in electrochemical processes.[25, 26] Graphene-based composite materials have been explored as next generation electrode materials for electrical and optical devices,[27] supercapacitors,[28] organic electronics[29] and dye-sensitized solar cells.[30] Graphene itself is considered a promising electrode material for a wide range of applications ranging from photocatalysis[31] to solar cells[24, 32] and optoelectronic devices.[33]

This article is protected by copyright. All rights reserved.

Author Manuscript

In electron microscopy, graphene is also advantageous for other reasons. Its mechanical properties and electron transparency make it ideal as the substrate in conventional TEM imaging[34], SEM and photoemission microscopy studies of liquid samples,[35, 36] and TEM imaging of liquid samples using graphene liquid cells[37] where the liquid is encapsulated between two graphene sheets for high-resolution imaging. Furthermore, graphene is thought to act as a scavenger for the radical species created during irradiation of water and aqueous solutions,[38, 39] which should in principle reduce electron beam effects on processes under observation. Graphene liquid cells (GLCs), and liquid cells composed of other 2D materials[40, 41] such as molybdenum disulfide (MoS_2), are excellent for high resolution imaging of suspended nanocrystals. However, these cells are not optimized for electrochemical experiments since the multiple closed pockets do not allow for patterned electrodes, liquid flow or a fixed and well-defined liquid geometry all of which are required for quantitative replication of processes important in electrochemistry, including diffusion.[5, 6, 15, 18] Advances in GLC design based on hybrids of graphene with silicon nitride[38, 42] or hexagonal boron nitride (hBN)[43] enable more control over liquid thickness and hence improved resolution over a larger area, compared to conventional GLCs. However, 2D materials have not been engineered into microfabricated liquid cell designs in a way that allows integration with electrodes or related functionality such as heating.[40]

Here, we demonstrate the integration of graphene and other 2D materials in electrochemical liquid cell TEM. We first develop a reproducible protocol in transferring 2D materials onto microfabricated liquid cell chips to achieve reliable electrical contacts and mechanical robustness. We then examine the suitability of 2D materials as electrodes by considering four different aspects. (1) We discuss 2D materials as suitable substrates on which to carry out electrodeposition by examining a well-characterized system, Cu deposition from an acidic electrolyte under cyclic voltammetry conditions. (2) We discuss wettability, to understand the physical processes at work when the electrolyte comes into contact with the 2D material. (3) We consider

This article is protected by copyright. All rights reserved.

Author Manuscript

stability to mechanical, electrical and beam damage, comparing graphene and TMDs such as tungsten diselenide (WSe_2) and MoS_2 of different thicknesses and growth methods. (4) We finally discuss resolution improvement, comparing graphene to Pt and other metal electrodes used in liquid cell electrochemistry. By combining imaging, electrochemical measurements and modelling, we show that multilayer graphene can serve as a low contrast and stable electrode material for electrodeposition, and can substantially improve the resolution for electrochemical quantification compared to Pt or other metal electrodes in liquid cell experiments.

2. Results and Discussion

2.1. Electrode Preparation and Electrochemical Deposition

Our standard electrochemical liquid cell chips incorporate three or more electrodes fabricated by lift-off patterning of a Pt layer 20 nm in thickness. The Pt surface outside the viewing window is coated with an insulating film to ensure that only an area a few tens of μm^2 is electrochemically active. We transferred exfoliated 2D materials onto these liquid cell chips using the process shown in Figure 1a (see transfer protocol in SI Section 1). Instead of conventional polymers that cannot be removed as effectively, we used cellulose acetate butyrate (CAB) to enhance the cleanliness in the transfer process.[44, 45] We transfered either a single 2D flake over one electrode – the working electrode, Figure 1b - or two and three separate flakes over working, reference and counter electrodes without short-circuiting (Figure 1c-d). If one or two flakes are used, an unmodified Pt electrode acts as a quasi-reference electrode. We have tested 2D flakes with areas 10^3 – $4x10^5$ μm^2 and irregular shapes. The thickness of the flake can be selected before transfer, down to single monolayer (ML) flakes, but we will show below that for mechanical stability of graphene, the optimum thickness is between ~3 and 15 layers (1-5 nm). Overall, this transfer process results in good electrical contact between Pt and graphene and good mechanical stability.

This article is protected by copyright. All rights reserved.

Author Manuscript

Transfer is compatible with the full functionalities of microfabricated liquid cells, such as biasing, heating, flowing and mixing capabilities. It is also possible to grow 2D materials by chemical vapor deposition (CVD) directly onto the window of the liquid cell chip, and we compare the grown and exfoliated films below.

To characterize the electrochemical performance of transferred graphene electrodes, we perform Cu electrodeposition under cyclic voltammetry (CV) conditions. The data in Figure 2a shows typical current peaks for diffusion-limited deposition (Equation 1) and stripping of Cu (Equation 2). We note that this imaging is carried out at a graphene edge that is located a few tens of micrometers away from the Pt electrode, so the graphene is able to provide a larger available area for imaging than the initial Pt electrode.

Cu clusters start to form (blue box, Figure 2a) at -0.14 V during the reverse scan. Nucleation and growth continue until the potential reaches -0.4 V and show characteristic diffusion-limited kinetics as the potential sweeps from -0.4 V to -0.2 V during the forward scan. At potentials of -0.2 V and more positive, the Cu clusters (orange box, Figure 2a) decrease in size rapidly and completely dissolve at -0.1 V. However, we note that one of the Cu clusters (Figure 2a, white arrow) behaves differently. It is associated with a ripple-like strain effect on graphene during the CV cycle and persists slightly longer than its neighbours. This may reflect a defect in the multilayer graphene and will be discussed in more detail below. Figures 2b-d show the potential, total charge passed and radius of representative clusters (labelled with coloured circles in the enlarged TEM image in Figure S2, *via* image analysis described in the Experimental Section).

The graphene electrode therefore enables nucleation, growth and stripping of copper. However some aspects of the experiment require further discussion. We first consider the voltage at the center of the CV loop. We find this to be around -300 mV with respect to the Pt quasi-reference electrode (Figure 2a). Prior experiments involving Cu or Au electrodes showed a CV that is centered

This article is protected by copyright. All rights reserved.

Author Manuscript

on zero V.[5] We attribute the difference to a combination of the open circuit potential (measured as described in SI Section 3), which shows a potential difference between Gr and Pt of typically ~<150 mV with respect to the Pt quasi-reference electrode, and the offset we measure between Cu and Pt of ~250-300 mV, shown in Figure S3. Note that if the initial Pt electrode is not fully covered by the transferred graphene (as in an example shown in Figure S4), deposition could take place on Pt and may even be preferred over graphene.[26, 36] In Figure 2 the graphene area (1200 μm^2) greatly exceeds the small area of exposed Pt (10 μm^2) and the CV characteristic resembles that for deposition on graphene rather than on Pt. More generally, for the most interpretable results it is helpful to place the graphene flake to cover the entire exposed Pt area.

The second interesting feature of the experiment is the slowdown in the island growth even at potentials where growth is expected to continue, Figure 2c, and the irreversible charge passed during the cycle, Figure 2d. We attribute both to the effects of depletion, which is well known to be important in liquid cell electrochemistry given the small volume of electrolyte present in the liquid cell.[5, 15, 46] It is possible to estimate roughly whether depletion will dominate the experiment. We first estimate from each image the total volume of copper deposited by that time, assuming that each island is hemispherical. Figure S5 shows the island size distribution at several times and Table S1 estimates the volume these islands represent. We then convert this “imaged volume” into a total volume deposited and charge passed, under the assumption that copper is deposited equally across the entire area of the electrode. (This assumption is hard to verify since much of the electrode area extends beyond the window and is therefore not visible.) We calculate the volume of electrolyte that is required to supply this number of copper ions, and hence the radius from which copper ions must have diffused. Finally, we compare this radius with the distance that copper ions are expected to diffuse, given their known diffusivity, at the time the image was recorded (Figure S6).

This article is protected by copyright. All rights reserved.

Author Manuscript

The conclusion, described in SI Section 4, is that we do indeed expect Cu^{2+} ion supply by diffusion to be unable to keep up with the deposition rate as the voltage continues to sweep to negative values. If diffusion depletes Cu ions around the electrode but voltage is still present, we expect other reactions such as gas formation to occur.[47] Such reactions would lead to discrepancy between the charge passed, calculated from the images as described above, and the charge passed based on the current *vs.* time plot. This is consistent with observations (SI Section 4). Parallel reactions would also generate irreversibility and a net charge flow after a complete CV cycle. Figure 2d indeed shows that -11 µC flows during deposition but +6.5 µC on stripping. The difference of -4.5 µC can be attributed to other reactions in the depleted solution.

These results demonstrate that the graphene electrode performs as expected in terms of enabling metal electrodeposition and stripping, given the depletion and diffusion limitations, which are a general issue in liquid cell microscopy that should be considered when setting up any electrochemical experiment. The electrode size and material, deposition rate and electrolyte composition remain important design criteria for achieving the most interpretable liquid cell electrochemistry measurements.

2.2 Wettability of 2D Materials

For quantitative analysis of electrochemical processes it is helpful for the liquid cell to be completely filled with electrolyte so that diffusion pathways through the liquid are well-defined. In experiments where the liquid does not fill the electrochemical cell completely, we often observe dramatic liquid motion during electrochemical cycling. Figure 3 shows images obtained during electrodeposition of Au on graphene under cyclic voltammetry conditions in an electrochemical liquid cell filled with 0.6 mM $HAuCl_4$ + 0.1 M HCl electrolyte. Dark patches, which are micrometer-

This article is protected by copyright. All rights reserved.

Author Manuscript

scale liquid droplets, move during forward and reverse sweeps. This phenomena occurred repeatedly in several sweeps.

We believe that this droplet motion is induced by the electric field and that it can provide information regarding wettability and filling of cells that include 2D materials. Graphene is known to be hydrophobic[48] when exposed to air for extended times, due to the attachment of airborne hydrocarbons. It has also been reported that graphene films show increased wettability upon application of voltage between water and graphene.[49] Theoretical works attribute the field-induced increase in wettability to the reorientation of dipoles along the applied electric field direction so as to attain a more energetically stable state and maximize hydrogen bond formation during water polarization.[50] Our *in situ* observations in Figure 3 are consistent with this picture. On mildly hydrophobic surfaces like graphene,[51] the dissolved metal ions tend to diffuse to the hydrophobic interface where they displace the water molecules to reduce the free energy and allow metal deposition on the surface. Graphene's high conductivity enables redistribution of the charges and dipoles at the solid-liquid interfaces so as to reduce the interfacial energy upon application of a potential, leading to an enhancement of surface wettability. The droplets we observe during *in situ* electrodeposition are likely the outcome of enhanced wettability induced by the electric field applied across the electrode. These results suggest a benefit of graphene as an electrode material: cycling may be used to improve wetting. A side benefit of graphene electrodes is that plasma cleaning is not required for creating wettable surfaces. The oxygen plasma treatment commonly used to improve the wettability of liquid cell interior surfaces works well for conventional chips with Pt and Au electrodes, but is less suitable for non-metal electrode materials such as glassy carbon that are prone to etching during plasma treatment (Figure S7a-b).

2.3 Mechanical and Electron Beam Effects in 2D Material Electrodes

We next discuss the mechanical and electrical stability of graphene and other 2D materials on liquid cell window chips. We compare materials of different thickness, as well as two methods of placing the 2D layers onto the SiN_x: exfoliation of flakes, as in the experiments shown in Figures 2-3, and growth of the 2D material directly onto the chip by chemical vapour deposition (CVD) (see Experimental Section).

Figure 4a shows MoS_2 flakes a few MLs thick on a SiN_x window chip imaged shortly after growth by CVD. The crystals are triangular and appear somewhat wrinkled, presumably due to cooling from the growth temperature. The liquid cell was filled with gold aurate solution and images were recorded during electron beam-induced growth of Au, Figure 4b. Striking changes are visible:

This article is protected by copyright. All rights reserved.

Author Manuscript

the triangle edges roll up into nanotube structures and Au nanoparticles form at these rolled edges, with some growing and others shrinking. It is known that dry CVD-grown MoS_2 flakes can roll up if liquid (ethanol) is added: the driving force is the high strain energy induced by thermal mismatch on cooling after growth.[52] The rolling up that we observe *in situ* takes place some time after liquid is introduced, but could be the result of liquid insertion between the MoS_2 and the substrate that reduces adhesion and stimulates a scrolling process.[52]

Our exfoliated films do not show scrolling, but evidence for the movement of liquid under the 2D layer is shown for both MoS_2 and WSe_2 in Figure 4d-f. This evidence comes from a deformation in the 2D layer associated with some of the beam-induced Au nanocrystals. The symmetric appearance in post-growth images (Figure 4e, f) suggest regions of mechanical strain as it is consistent with the distinctive bend contours seen when 2D materials are deformed over particles and curve due to van der Waals interactions.[53] We observe similar bend contours in graphene electrodes (Figure S8), mainly when the graphene layer is thick (> 30 layers) but much less commonly when it is thin. We speculate that defects in the 2D materials serve to preferentially nucleate metal nanocrystals that grow in liquid that has penetrated to the 2D material/SiN_x interface, deforming the 2D layer. The contrast in Figure 2a (white arrow) is likely the outcome of the same phenomenon for an electrochemically generated nanoparticle. Although mechanical compliance around deposited material is not a usual feature for an electrode material, we suggest that this could be an advantage if we think of it as an additional control knob to mechanically shape metal nanostructures during electrodeposition by leveraging van der Waals interactions.

Apart from this occasional bending around nanocrystals, we find that exfoliated graphene can be mechanically robust as an electrode material. However, the thickness of the exfoliated film is critical. Figure S9a-c shows that exfoliated electrodes with thickness ranging from 12 to 15 layers can be stable for several days without showing significant tearing or scrolling after *in situ*

This article is protected by copyright. All rights reserved.

Author Manuscript

electrochemical stressing. As mentioned above, thicker graphene (>30 layers) has a tendency to form pocket-like structures while thin graphene (1-2 layers) tends to detach from the metal electrode after electrochemical stressing (Figure S9d-f).

We expect electron beam effects to play a role in the stability of electrodes composed of 2D materials, since it is well known that these materials suffer from knock-on damage when irradiated with high voltage electrons. The effect of irradiation on graphene adjacent to liquid has been discussed in the graphene liquid cell literature. Electron flux in the range 360-800 $e^-/Å^2 \cdot s$ do not lead to visible damage of the graphene[38, 54] although at higher doses drying of the liquid within the pockets has been noted. Our experiments used lower flux, below 30 $e^-/Å^2 \cdot s$ and consistent with the literature, we did not observe visible damage to the several ML-thick electrode (although 1-3 ML graphene layers can show etching under extended irradiation). However, atomic scale damage, such as from individual knock-on events, would not be visible through the liquid and SiN. A more sensitive measure of damage is the electrochemical performance of the electrode. Repeated deposition and stripping of Cu is shown in Figure S10. Nucleation sites generally repeat,[4] but after several minutes of irradiation nuclei also form at new sites. If irradiation can induce nucleation sites, dose should be minimized even in the regime where there is no visible damage. We also note that reaction of graphene with water radiolysis products is reported to form graphene oxide.[38] In our experiments, we do not observe effects that might suggest formation of an insulating layer.[55]

The electron beam drives other reactions, including the beam-induced deposition of metal nanocrystals shown in Figure 4, which occurs above a threshold electron flux (Figure S11). The low flux used in Figure 2 was chosen to minimize this effect, and the electrodeposition occurs similarly with and without irradiation (Figure S12). However, beam effects on electrochemistry may be more complex than beam-induced deposition alone. Irradiation can cause both growth and etching of nanoparticles, depending on the balance between the concentrations of oxidizing and reducing

This article is protected by copyright. All rights reserved.

Author Manuscript

radiolytic species.[13] Furthermore, graphene is a well-known scavenger of hydroxyl radicals.[38] We may expect the presence of graphene to shift the balance towards deposition by lowering the hydroxyl radical concentration. A qualitative description of these effects is given in SI Section 8. Quantifying these effects requires calculations that include the complexity of the chemical environment as well as diffusion and nucleation. However, we are intrigued by the possibility that graphene's scavenging properties may provide an additional pathway for control of liquid cell electrochemistry.

We finally discuss the electrical stability of graphene compared to other 2D materials. In Figure 4g, a thick WSe_2 electrode exhibited structural instability during cycling (Figure 4h) and eventually broke down after several CV scans (Figure 4i). In contrast, graphene electrodes showed electrical stability in various acidic electrolytes. For example, Figure S14 shows that it is stable up to ±900 mV (with respect to Pt-quasi reference electrode) in 0.1 M H_2SO_4 and Figure 3 shows stability to ±1.5 V in 0.6 mM $HAuCl_4$ + 0.1 M HCl. This is close to values reported in literature where graphene is stable within the potential window -0.8 V to +2 V *vs.* Ag/AgCl before undergoing oxidation to graphene oxide.[56]

2.4 Potential Distribution at 2D Material Electrodes

Interpreting liquid cell electrochemical data requires knowledge of how the potential varies across the electrode since any potential drop due to the resistivity of the electrode material could affect the lateral distribution of the electrochemical reactions. We first note that an equivalent circuit model for resistance mapping (Figure S15) suggests that the interface cleanliness, number and planarity of graphene layers are important in determining the overall resistivity of the Pt-graphene system and, given the other sources of resistance in the liquid cell, the addition of graphene is not expected to change the voltage at the electrode surface significantly.

This article is protected by copyright. All rights reserved.

Author Manuscript

To achieve a more accurate evaluation of the lateral distribution of potential across the Pt/graphene and Pt/WSe_2 electrochemical liquid cell systems, we used finite element analysis to map the potential and electric field via a simplified 2D Stationary model in COMSOL Multiphysics.[57] To choose a resistivity value for the graphene, factors such as the doping level, substrate and defects should be included. Multilayer graphene/graphite resistivities are reported in the range 10^{-8} - 10^{-6} Ωm.[58] Our multilayer graphene (>7 L) approaches a bulk properties approximation[59] and we use an average of these literature values. For WSe_2 the resistivity is several orders of magnitude higher (~10^{-3} Ωm)[60]. For the electrolyte, we do not include the electrical double layer as the 2D model geometry can not account for the out-of-plane potential profile governed by the electrical double layer. The resistivity of the electrolyte is ~1 x 10^{-4} Ωm, (SI Section 10) so it dominates the resistivity of the graphene but not the WSe_2. We assume quasi-static equilibrium, with the initial voltage of the working electrode set at 0.1 V and the counter electrode grounded. As expected, the potential drop is much larger across the WSe_2 electrode than the graphene electrode (Figure 5a-c). The potential is almost constant across the graphene flake (voltage drop < 1 mV), whereas the WSe_2 potential drops significantly (~70 %) from the value at the Pt contact, a varying potential that could complicate interpretation of electrochemical data (Figure 5c). The small lateral variation in potential across even large graphene working electrodes (Figure 5f) is consistent with our experiments in which deposition on graphene electrodes occurs across tens of µm from the Pt electrode. A final feature from these simulations is the prediction of electrochemical 'hotspots' in the form of increased electric field at the corners of the 2D flakes (Figure 5d-e). Since exfoliated flakes exhibit uncontrolled geometries, it is important to consider this electric field non-uniformity on a case-by-case basis. This simple analysis should be taken to highlight the qualitative difference between graphene and WSe_2 electrodes. More quantitative results would require a 3D simulation, but it is evident that a high conductivity is important for liquid cell electrodes, and the electrical performance of graphene is superior to less conductive 2D materials such as WSe_2.

This article is protected by copyright. All rights reserved.

Author Manuscript

2.5 Resolution Enhancement

The final aspect we consider for an electrode material in liquid cell electrochemistry is the achievable image resolution. High spatial resolution has been a key driving force behind development of liquid cell TEM. Conventional electrode choices such as Pt and Cu polycrystalline film contribute a large mass contrast. The presence of additional material in the beam path reduces the ability to discriminate small islands of material above (Figure S2, S7c-e, S8b). In conditions where the resolution is dose-limited, as is frequently the case in liquids, the resolution of an object depends on its contrast. For bright field imaging conditions this is essentially dependent on the mass thickness of the object in comparison to the mass thickness of all the other components in the electrochemical cell. In electrochemical experiments the components include the windows, liquid layer and electrodes.[12] We can assess the expected resolution for an object growing on a given electrode material by comparing the mass thickness contribution as described by Equation 3.

Here, d_m gives the resolution of liquid samples and mass thickness is the product of thickness (t) and density (ρ). In SI Section 11 we compare mass thickness values for liquid cells with an electrode of 0.7 - 6 nm graphene (~2-20 layers) versus 20 nm thick Pt (or Au), as is often used in microfabricated chips. The liquid cell includes a 50 nm SiN_x top membrane, 200 nm thick water and 30 nm SiN_x bottom membrane. We find that the mass thicknesses have a ratio $d_{m,Gr}/d_{m,Pt} \approx 2$. This suggests that the resolution is significantly improved by a factor of 2 using a graphene electrode rather than Pt layer, under the conditions where mass thickness is the limiting factor.

3. Conclusion

We have shown that 2D material electrodes can be integrated with microfabricated liquid cell chips using a reproducible transfer protocol to achieve reliable electrical contact and mechanical robustness. Through *in situ* electrochemical experiments, we demonstrate that graphene in particular can be used as an electrode to enable quantitative electrochemical metal deposition studies. Combining electrochemical analysis with *in situ* imaging can improve our understanding of

This article is protected by copyright. All rights reserved.

Author Manuscript

the nucleation sites, growth mechanisms and structures formed during electrochemical reactions that take place on the surface of an electrode. The use of graphene as an electrode material reduces mass contrast, and therefore improves the spatial resolution for such electrochemical quantification, compared to conventional Pt or other metal electrodes often used in liquid cell experiments. Our observations reveal that graphene has other key benefits. The enhanced wettability induced by the electric field across the Pt/graphene hybrid electrode system is advantageous for controlled electrodeposition. The remarkable mechanical and electrical properties of graphene lead to high stability in our experiments during electrochemical cycling. It is even possible that the scavenging properties of graphene may improve the beam sensitivity of the electrochemical experiment. Combining graphene with a microfabricated liquid cell chip is a more complex process than creating a GLC, but the lifetime of the graphene electrode electrochemical liquid cell is significantly improved compared to conventional GLCs in which the liquid pocket typically dries out within 2-3 min.[54] Our modelling of the performance of our hybrid electrode system shows that the low resistivity and therefore minimal potential drop across the graphene is an important factor in establishing conductivity and chemical stability during electrochemical reactions.

Overall, the combination of *in situ* imaging, electrochemical measurement and modelling demonstrates that graphene is a promising electrode material that can provide an electron beam-stable and low contrast extended electrode area for electrodeposition at improved image resolution. Further exploration of the possibilities of graphene and other conductive 2D materials as electrode materials in liquid cell TEM opens up new opportunities for addressing a wide range of electrochemical problems. We are particularly excited by the possibilities of patterning the shapes and sizes of flakes before exfoliation; by controlling nucleation and growth in electrochemical processes by using patterned surfaces or scrolls; the enhanced information that can result from a low contrast and uniform electrode, and the opportunities to perform experiments where the

This article is protected by copyright. All rights reserved.

Author Manuscript

electrode material is relevant to electrochemical processes involving energy storage and electrocatalysis.

4. Experimental Section

Sample preparation: Sulfuric acid (Cat. No. 1090721000-1L, EMD Milipore Co., Billerica, MA, USA), hydrochloric acid (Cat. No. 87003-500 ML, VWR Co., Radnor, PA, USA), copper sulfate (Cat. No. 451657-10G, Sigma-Aldrich Co., St Louis, MO, USA), gold (III) chloride trihydrate (Cat. No. 520918-1G, Sigma-Aldrich Co., St Louis, MO, USA), molybdenum (VI) oxide (Cat. No. 267856-100G, Sigma-Aldrich Co., St Louis, MO, USA), and sulphur (Cat. No. 84683-1KG, Sigma-Aldrich Co., St Louis, MO, USA) were used as received without further purification. All aqueous solutions were prepared using deionized water.

Experimental procedures: For *in situ* electrochemical cell experiments, each electrochemical cell consisted of one 100 nm-spacer chip with ultrathin (30 nm-thick) electron translucent SiN_x membranes windows (Hummingbird Scientific, Lacey, WA, USA) and a modified electrochemical chips that had 2D materials transferred directly on top of the 50 nm-thick SiN_x membrane window (Hummingbird Scientific, Lacey, WA, USA). Before assembling the electrochemical cell, we cleaned the surface of SiN_x membrane windows with an oxygen plasma for 1 minute to render their surfaces hydrophilic. Each electrochemical cell was assembled and loaded into an analytical flow holder (Hummingbird Scientific, Lacey, WA, USA). After checking and confirming that there are no leaks in the flow cell, the holder was inserted into a JEOL 2011 TEM operated at 200 kV for *in situ* imaging where the incident electron flux ranged from 10 to 30 $e^-/(Å^2 \cdot s)$. Image series were acquired at 10-30 frames per second using an AMT camera (AMT Imaging, Woburn, MA, USA). We introduced the mixed acid and metal salt solution (0.1 M HCl or 0.1 M H_2SO_4 and $CuSO_4$, $HAuCl_4$) into the liquid cell *via* a flow tube (diameter of 200 µm and length of 50 cm) connected to a syringe pump, using a flow

This article is protected by copyright. All rights reserved.

Author Manuscript

rate of 5 μL/min. It takes a few minutes for the solution to reach the window area of the electrochemical cell. On the videos, t = 0 s corresponds to application of voltage to the electrodes. The electrochemical measurements used a Gamry Reference 600+ potentiostat (Gamry Instruments, Pennsylvania, USA). Post-deposition high resolution TEM (HAADF-STEM) imaging and diffraction analysis were performed with a JEOL 2010F operated at 200 kV. All aqueous solutions were prepared using deionized water without further purification.

2D Materials exfoliation: Thermally grown 90 nm SiO_2/Si wafers were pre-treated with oxygen plasma and the 2D material (Gr, MoS_2, or WSe_2) was mechanically exfoliated onto them using conventional Scotch tape method. Graphene flakes were obtained from NGS Graphite (NGS Trading and Consulting GmbH, Leinburg, Germany), while MoS_2 and WSe_2 flakes were obtained from HQ Graphene (HQ graphene, Groningen, The Netherlands). Flakes of suitable thickness were then identified by their contrast in optical microscopy. The transfer protocol is a wedging transfer process to suspend 2D materials on TEM chips, building on the procedure in Ref.[44], and described further in Ref.[45] and SI Section 1.

Chemical Vapor Deposition (CVD) of MoS_2: Molybdenum (VI) oxide (15 mg of MoO_3) and sulfur (150 mg of S) precursors in separate alumina crucibles were loaded into the 1-inch quartz tube furnace. The liquid cell spacer chip was placed above the MoO_3 crucible. The growth temperature was set to 795 ℃ at a ramp rate of 20 ℃/min. Once the temperature reached the pre-set growth temperature, sulfur precursor was inserted to heating zone and the flow rate of carrier gas (Ar, 99.5%) was adjusted from 200 sccm (cm^3/min) to 10 sccm. After growing for 7 minutes, the lid of CVD furnace was opened. The spacer chip was taken out from the furnace after cooling down for 30 minutes.

Image processing: The area of islands shown in Figure 2 were obtained by image analysis performed on individual image sequences taken from TEM movies in in Python 3.7[61] using the libraries numpy,[62] opencv[63] and matplotlib.[64] Individual images (frames) are imported as 8-bit grayscale (0

This article is protected by copyright. All rights reserved.

Author Manuscript

to 255) matrix. Data are smoothed and salt-and-pepper noise is reduced by using a bilateral filter with a diameter of 9. The contours of individual islands are determined in the filtered images by using a binary threshold and contours are obtained using the provided canny edge detection function available in the opencv[63] library. The corresponding area of each island is straightforwardly obtained from the number of pixels enclosed by each contour for every movie frame.

Finite-Element Method Simulation: The geometry was defined as a 200 µm x 50 µm rectangular SiN_x window, an irregular polygon shape as the 2D material, and three Pt electrodes that extend onto the window set as working, reference, and counter electrode, respectively. The height of the electrodes extended to the SiN_x window was 2 µm (*i.e.*, y =2 µm in Figure 5), and the widths were 10 µm, 5 µm and 20 µm with a 5 µm gap between each electrode. The electrolyte was simulated with the material properties of 0.1 M H_2SO_4 (in which H^+ and SO_4^{2-} are the charge carriers).[65] For the electrodes we used properties of Pt solid,[66] and a polygon with material properties of graphene[67] or WSe_2[68]. Static electrolyte condition with negligible convection[15] is considered in our modelling. A physics controlled mesh was set with a 'normal' element size, with automatic mesh refinement at the boundaries. The outer edges of the chip were set to be electrically insulated, and the remainder of the interior boundaries to the continuity condition.

Supporting Information

Supporting Information is available from the Wiley Online Library or from the author.

Acknowledgements

This work made use of facilities and instrumentation supported by NSF through the Massachusetts Institute of Technology Materials Research Science and Engineering Center under Grant (DR-1419807). K. R. acknowledges funding from the MIT MathWorks Engineering Fellowship. J. K. acknowledges support by the Alexander von Humboldt foundation. The authors would like to acknowledge the Lord Foundation of Massachusetts for financial support.

Received: ((will be filled in by the editorial staff))
Revised: ((will be filled in by the editorial staff))
Published online: ((will be filled in by the editorial staff))

This article is protected by copyright. All rights reserved.

Author Manuscript

References

[1] K. Petersen, "A new age for MEMS", presented at *The 13th International Conference on Solid-State Sensors, Actuators and Microsystems, 2005. Digest of Technical Papers. TRANSDUCERS '05.*, 5-9 June 2005, 2005.

[2] N. Hodnik, G. Dehm, K. J. J. Mayrhofer, Acc. Chem. Res. 2016, 49, 2015.

[3] B. L. Mehdi, J. Qian, E. Nasybulin, C. Park, D. A. Welch, R. Faller, H. Mehta, W. A. Henderson, W. Xu, C. M. Wang, J. E. Evans, J. Liu, J. G. Zhang, K. T. Mueller, N. D. Browning, Nano Lett. 2015, 15, 2168.

[4] M. J. Williamson, R. M. Tromp, P. M. Vereecken, R. Hull, F. M. Ross, Nat Mater 2003, 2, 532.

[5] A. Radisic, P. M. Vereecken, J. B. Hannon, P. C. Searson, F. M. Ross, Nano Lett. 2006, 6, 238.

[6] A. Radisic, F. M. Ross, P. C. Searson, The Journal of Physical Chemistry B 2006, 110, 7862.

[7] E. R. White, S. B. Singer, V. Augustyn, W. A. Hubbard, M. Mecklenburg, B. Dunn, B. C. Regan, ACS Nano 2012, 6, 6308; J. M. Murbach, S. Currlin, A. Widener, Y. Tong, S. Chhatre, V. Subramanian, D. C. Martin, B. N. Johnson, K. J. Otto, MRS Communications 2018, 8, 1043.

[8] Z. Zeng, W.-I. Liang, H.-G. Liao, H. L. Xin, Y.-H. Chu, H. Zheng, Nano Lett. 2014, 14, 1745; C. Hou, J. Han, P. Liu, C. Yang, G. Huang, T. Fujita, A. Hirata, M. Chen, Advanced Energy Materials 2019, 9, 1902675; R. L. Sacci, N. J. Dudney, K. L. More, L. R. Parent, I. Arslan, N. D. Browning, R. R. Unocic, Chem. Commun. 2014, 50, 2104.

[9] D. Lee, H. Park, Y. Ko, H. Park, T. Hyeon, K. Kang, J. Park, J. Am. Chem. Soc. 2019, 141, 8047; C. Hou, J. Han, P. Liu, C. Yang, G. Huang, T. Fujita, A. Hirata, M. Chen, Nano Energy 2018, 47, 427; L. Lutz, W. Dachraoui, A. Demortiere, L. Johnson, P. Bruce, A. Grimaud, J.-M. Tarascon, Nano Lett. 2018, 18; K. He, X. Bi, Y. Yuan, T. Foroozan, B. Song, K. Amine, J. Lu, R. Shahbazian-Yassar, Nano Energy 2018, 49, 338; J. J. Lodico, M. Mecklenburg, H. L. Chan, W. A. Hubbard, B. C. Regan, Microsc. Microanal. 2019, 25, 2060; J. H. Chang, J. Y. Cheong, S. J. Kim, Y.-S. Shim, J. Y. Park, H. K. Seo, K. S. Dae, C.-W. Lee, I.-D. Kim, J. M. Yuk, ACS Omega 2019, 4, 6784; O. M. Karakulina, A. Demortière, W. Dachraoui, A. M. Abakumov, J. Hadermann, Nano Lett. 2018, 18, 6286.

[10] V. Beermann, M. E. Holtz, E. Padgett, J. F. de Araujo, D. A. Muller, P. Strasser, Energy Environ. Sci. 2019, 12, 2476; J. Yang, S. Prabhudev, C. M. Andrei, G. A. Botton, L. Soleymani, Chem. Commun. 2019, 55, 9204; S. F. Tan, S. W. Chee, Z. Baraissov, H. Jin, T. L. Tan, U. Mirsaidov, The Journal of Physical Chemistry Letters 2019, 10, 6090; N. Ortiz Peña, D. Ihiawakrim, M. Han, B. Lassalle-Kaiser, S. Carenco, C. Sanchez, C. Laberty-Robert, D. Portehault, O. Ersen, ACS Nano 2019, 13, 11372; S. Nagashima, T. Ikai, Y. Sasaki, T. Kawasaki, T. Hatanaka, H. Kato, K. Kishita, Nano Lett. 2019, 19, 7000.

[11] J. Yang, C. M. Andrei, Y. Chan, B. L. Mehdi, N. D. Browning, G. A. Botton, L. Soleymani, Langmuir 2019, 35, 862; G.-Z. Zhu, S. Prabhudev, J. Yang, C. M. Gabardo, G. A. Botton, L. Soleymani, The Journal of Physical Chemistry C 2014, 118, 22111.

This article is protected by copyright. All rights reserved.

Author Manuscript

[12] N. de Jonge, F. M. Ross, Nat Nano 2011, 6, 695; N. de Jonge, L. Houben, R. E. Dunin-Borkowski, F. M. Ross, Nature Reviews Materials 2019, 4, 61.

[13] N. M. Schneider, M. M. Norton, B. J. Mendel, J. M. Grogan, F. M. Ross, H. H. Bau, The Journal of Physical Chemistry C 2014, 118, 22373.

[14] T. J. WOEHL, P. ABELLAN, J. Microsc. 2017, 265, 135.

[15] N. M. Schneider, J. H. Park, J. M. Grogan, D. A. Steingart, H. H. Bau, F. M. Ross, Nature Communications 2017, 8, 2174.

[16] S. Cherevko, A. R. Zeradjanin, A. A. Topalov, N. Kulyk, I. Katsounaros, K. J. J. Mayrhofer, ChemCatChem 2014, 6, 2219.

[17] L. Wang, J. Wen, H. Sheng, D. J. Miller, Nanoscale 2016, 8, 17250.

[18] R. R. Unocic, R. L. Sacci, G. M. Brown, G. M. Veith, N. J. Dudney, K. L. More, F. S. Walden, D. S. Gardiner, J. Damiano, D. P. Nackashi, Microsc. Microanal. 2014, 20, 452.

[19] L. Coustan, G. Shul, D. Bélanger, Electrochem. Commun. 2017, 77, 89.

[20] M. Weissmann, S. Baranton, J.-M. Clacens, C. Coutanceau, Carbon 2010, 48, 2755.

[21] R. G. Gordon, MRS Bull. 2000, 25, 52.

[22] M. A. Martínez, J. Herrero, M. T. Gutiérrez, Electrochim. Acta 1992, 37, 2565.

[23] D. J. Hynek, J. V. Pondick, J. J. Cha, APL Materials 2019, 7, 030902; K. S. Kumar, N. Choudhary, Y. Jung, J. Thomas, ACS Energy Letters 2018, 3, 482; S. J. Kim, K. Choi, B. Lee, Y. Kim, B. H. Hong, Annual Review of Materials Research 2015, 45, 63.

[24] F. Bonaccorso, L. Colombo, G. Yu, M. Stoller, V. Tozzini, A. C. Ferrari, R. S. Ruoff, V. Pellegrini, Science 2015, 347, 1246501.

[25] D. A. C. Brownson, C. E. Banks, Analyst 2010, 135, 2768; M. Pumera, Chem. Soc. Rev. 2010, 39, 4146.

[26] D. A. C. Brownson, C. E. Banks, The Handbok of Graphene Electrochemistry 2014.

[27] G. Jo, M. Choe, S. Lee, W. Park, Y. H. Kahng, T. Lee, Nanotechnology 2012, 23, 112001.

[28] Q. Ke, J. Wang, Journal of Materiomics 2016, 2, 37.

[29] S. Pang, Y. Hernandez, X. Feng, K. Müllen, Adv. Mater. 2011, 23, 2779.

[30] H. Wang, Y. H. Hu, Energy Environ. Sci. 2012, 5, 8182.

[31] B. Luo, G. Liu, L. Wang, Nanoscale 2016, 8, 6904.

This article is protected by copyright. All rights reserved.

Author Manuscript

[32] M. M. Tavakoli, G. Azzellino, M. Hempel, A.-Y. Lu, F. J. Martin-Martinez, J. Zhao, J. Yeo, T. Palacios, M. J. Buehler, J. Kong, Adv. Funct. Mater., 2020, 2001924.

[33] M. Chhowalla, D. Jena, H. Zhang, Nature Reviews Materials 2016, 1, 16052.

[34] P. Y. Huang, J. C. Meyer, D. A. Muller, MRS Bull. 2012, 37, 1214.

[35] A. Yulaev, H. Guo, E. Strelcov, L. Chen, I. Vlassiouk, A. Kolmakov, ACS Applied Materials & Interfaces 2017, 9, 26492; J. D. Stoll, A. Kolmakov, Nanotechnology 2012, 23, 505704; C. H. Wu, R. S. Weatherup, M. B. Salmeron, PCCP 2015, 17, 30229; L. J. Falling, R. V. Mom, L. E. Sandoval Diaz, S. Nakhaie, E. Stotz, D. Ivanov, M. Hävecker, T. Lunkenbein, A. Knop-Gericke, R. Schlögl, J.-J. Velasco-Vélez, ACS Applied Materials & Interfaces 2020, 12, 37680; J. J. Velasco-Velez, V. Pfeifer, M. Hävecker, R. S. Weatherup, R. Arrigo, C.-H. Chuang, E. Stotz, G. Weinberg, M. Salmeron, R. Schlögl, A. Knop-Gericke, Angew. Chem. Int. Ed. 2015, 54, 14554.

[36] S. Nemšák, E. Strelcov, T. Duchoň, H. Guo, J. Hackl, A. Yulaev, I. Vlassiouk, D. N. Mueller, C. M. Schneider, A. Kolmakov, J. Am. Chem. Soc. 2017, 139, 18138.

[37] J. M. Yuk, J. Park, P. Ercius, K. Kim, D. J. Hellebusch, M. F. Crommie, J. Y. Lee, A. Zettl, A. P. Alivisatos, Science 2012, 336, 61; M. Textor, N. de Jonge, Nano Lett. 2018, 18, 3313.

[38] H. Cho, M. R. Jones, S. C. Nguyen, M. R. Hauwiller, A. Zettl, A. P. Alivisatos, Nano Lett. 2017, 17, 414.

[39] Y. Qiu, Z. Wang, A. C. E. Owens, I. Kulaots, Y. Chen, A. B. Kane, R. H. Hurt, Nanoscale 2014, 6, 11744.

[40] S. M. Ghodsi, C. M. Megaridis, R. Shahbazian-Yassar, T. Shokuhfar, Small Methods 2019, 3, 1900026.

[41] J. Yang, M. K. Choi, Y. Sheng, J. Jung, K. Bustillo, T. Chen, S.-W. Lee, P. Ercius, J. H. Kim, J. H. Warner, E. M. Chan, H. Zheng, Nano Lett. 2019, 19, 1788.

[42] H. Rasool, G. Dunn, A. Fathalizadeh, A. Zettl, physica status solidi (b) 2016, 253, 2544; I. N. Dahmke, A. Verch, J. Hermannsdörfer, D. B. Peckys, R. S. Weatherup, S. Hofmann, N. de Jonge, ACS Nano 2017, 11, 11108.

[43] D. J. Kelly, M. Zhou, N. Clark, M. J. Hamer, E. A. Lewis, A. M. Rakowski, S. J. Haigh, R. V. Gorbachev, Nano Lett. 2018, 18, 1168.

[44] G. F. Schneider, V. E. Calado, H. Zandbergen, L. M. K. Vandersypen, C. Dekker, Nano Lett. 2010, 10, 1912.

[45] K. Reidy, G. Varnavides, J. D. Thomsen, A. Kumar, T. Pham, A. M. Blackburn, P. Anikeeva, P. Narang, J. M. LeBeau, F. M. Ross, Nature Communications 2021, 12, 1290.

[46] F. M. Ross, in *Liquid Cell Electron Microscopy*, (Ed: F. M. Ross), Cambridge University Press, Cambridge 2016, 210.

This article is protected by copyright. All rights reserved.

Author Manuscript

[47] Y. Li, J. Z. Sun, C. Bian, J. H. Tong, H. P. Dong, H. Zhang, S. H. Xia, AIP Advances 2015, 5, 041312.

[48] Z. Li, Y. Wang, A. Kozbial, G. Shenoy, F. Zhou, R. McGinley, P. Ireland, B. Morganstein, A. Kunkel, S. P. Surwade, L. Li, H. Liu, Nature Materials 2013, 12, 925; M. E. Schrader, The Journal of Physical Chemistry 1975, 79, 2508.

[49] J. Pu, S. Wan, Z. Lu, G.-a. Zhang, L. Wang, X. Zhang, Q. Xue, Journal of Materials Chemistry A 2013, 1, 1254.

[50] M. Islam, M. M. Rahman, M. M. Chowdhury, M. K. Alam, ACS Applied Nano Materials 2019, 2, 5857; X. Guo, J. Su, H. Guo, Soft Matter 2012, 8, 1010.

[51] M. Munz, C. E. Giusca, R. L. Myers-Ward, D. K. Gaskill, O. Kazakova, ACS Nano 2015, 9, 8401.

[52] X. Cui, Z. Kong, E. Gao, D. Huang, Y. Hao, H. Shen, C.-a. Di, Z. Xu, J. Zheng, D. Zhu, Nature Communications 2018, 9, 1301.

[53] S. M. G.-A. Rehn, Theodor M.; Qiao, Liang; Jones, Matthew R. , ChemRxiv. Preprint 2020.

[54] M. R. Au - Hauwiller, J. C. Au - Ondry, A. P. Au - Alivisatos, JoVE 2018, e57665; M. R. Hauwiller, J. C. Ondry, C. M. Chan, P. Khandekar, J. Yu, A. P. Alivisatos, J. Am. Chem. Soc. 2019, 141, 4428; M. R. Hauwiller, X. Ye, M. R. Jones, C. M. Chan, J. J. Calvin, M. F. Crook, H. Zheng, A. P. Alivisatos, ACS Nano 2020, 14, 10239.

[55] S. Y. Lim, W. Shen, Z. Gao, Chem. Soc. Rev. 2015, 44, 362.

[56] A. Ambrosi, C. K. Chua, A. Bonanni, M. Pumera, Chem. Rev. 2014, 114, 7150.

[57] E. J. F. Dickinson, H. Ekström, E. Fontes, Electrochem. Commun. 2014, 40, 71.

[58] H. O. Pierson, *Handbook of carbon, graphite, diamond, and fullerenes : properties, processing, and applications*, Noyes Publications, Park Ridge, N.J., U.S.A. 1993.

[59] K. Ito, M. Katagiri, T. Sakai, Y. Awano, Jpn. J. Appl. Phys. 2013, 52, 06GD08.

[60] K. Kam, in *Physics and Astronomy*, Vol. Doctor of Philosophy, Iowa State University, 1982.

[61] T. E. Oliphant, Computing in Science & Engineering 2007, 9, 10.

[62] S. v. d. Walt, S. C. Colbert, G. Varoquaux, Computing in Science & Engineering 2011, 13, 22.

[63] G. Bradski, Dr. Dobb's Journal of Software Tools 2000.

[64] J. D. Hunter, Computing in Science & Engineering 2007, 9, 90.

[65] E. Koposova, A. Kisner, G. Shumilova, Y. Ermolenko, A. Offenhäusser, Y. Mourzina, The Journal of Physical Chemistry C 2013, 117, 13944.

This article is protected by copyright. All rights reserved.

[66] D. R. Lide, *CRC handbook of chemistry and physics: a ready-reference book of chemical and physical data*, CRC Press, Boca Raton, Fla 2003.

[67] H. O. Pierson, 1993; J. Fang, W. G. Vandenberghe, M. V. Fischetti, PhRvB 2016, 94, 045318.

[68] L. H. Brixner, J. Inorg. Nucl. Chem. 1962, 24, 257; Z. Huang, W. Zhang, W. Zhang, Materials 2016, 9, 716.

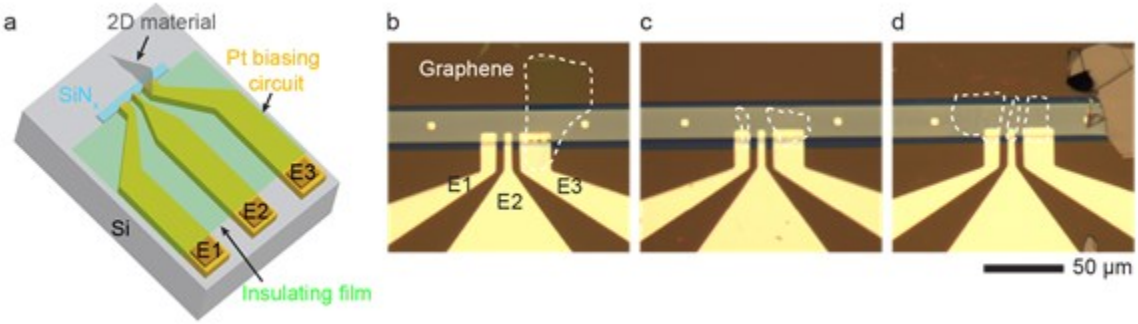

Figure 1: **2D material/Pt hybrid electrode structures.** (**a**) Schematic view of a commercially available biasing chip with 20-nm thick Pt electrodes (yellow) crossing the viewing window (cyan) and connected to three contact pads E1, E2 and E3 that can be assigned as counter, reference and working electrodes respectively. An insulating layer (green) passivates the surface of the electrodes with an exception of the area that lies on the viewing window. A 2D flake is shown as the irregular grey polygon. (**b-d**) Light microscope images showing biasing chips on which flakes (dotted white lines) are transferred over the working electrode, working and counter electrodes and working, reference and counter electrodes respectively.

Author Manuscript

This article is protected by copyright. All rights reserved.

Author Manuscript

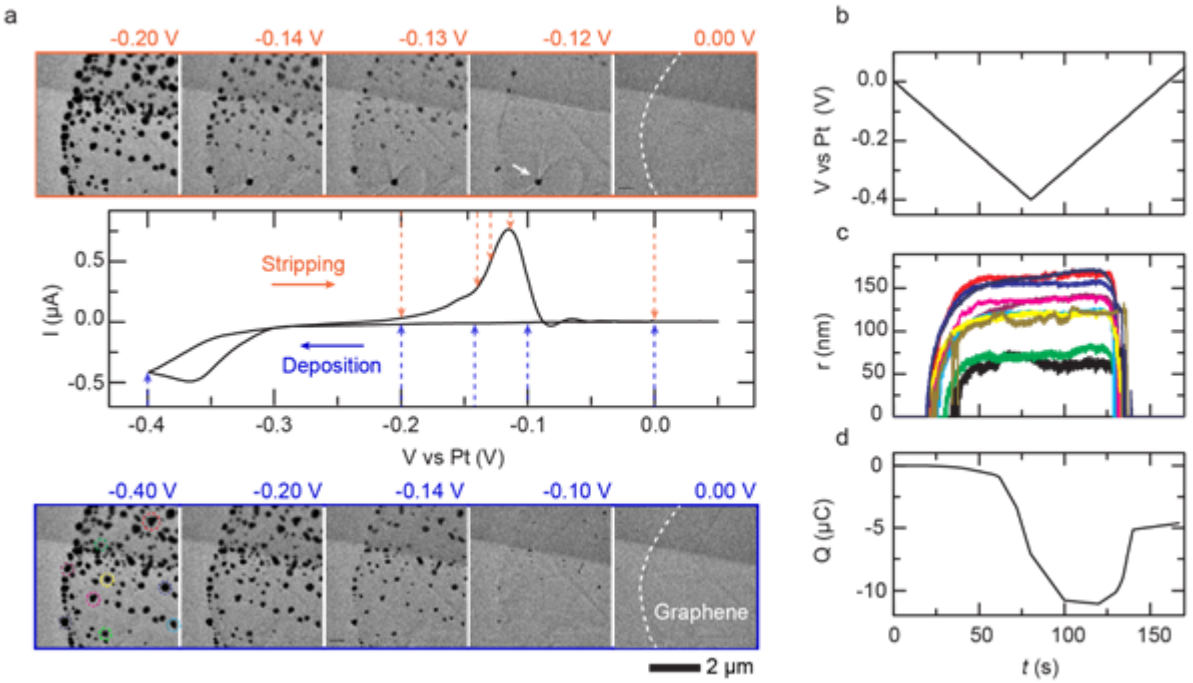

Figure 2: **Cyclic voltammetry (CV) of Cu in 0.1 M $CuSO_4$ + 0.1 M H_2SO_4 electrolyte.** (**a**) Images from a TEM video (Supporting video 1) obtained with electron flux of 3 $e^-/Å^2 \cdot s$ during a CV cycle scanning from 0 V to -0.4 V to +0.05 V at 5 mV/s using the electrochemical liquid cell with electrode geometry shown in Figure 1c. The potential for each image is indicated by dotted lines with deposition in blue and stripping in orange. (**b, c**) Potential and radius of representative clusters. Colors correspond to the circles in the image at -0.4 V which is enlarged in Figure S2 to show details. (**d**) Accumulated charge *vs.* time, extracted by integrating the current during the CV cycle.

This article is protected by copyright. All rights reserved.

Author Manuscript

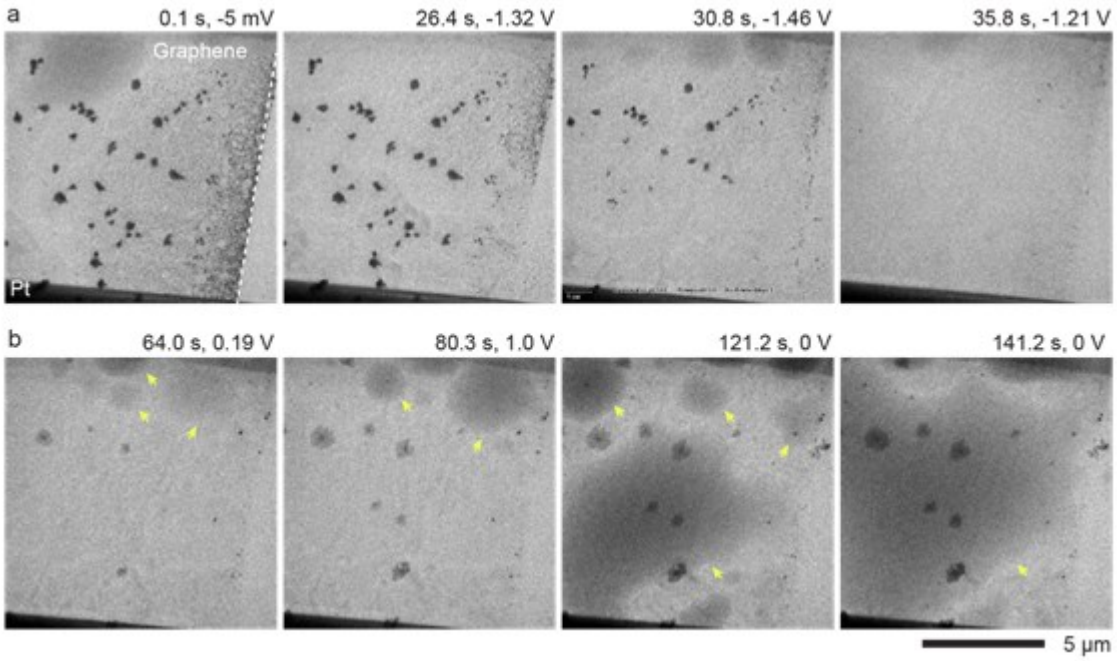

Figure 3: Electric-field induced increase in wettability of 2D materials. *In situ* TEM images showing (**a**) stripping and (**b**) growth of Au on graphene (edge shown with a dotted line) at the graphene/Pt working electrode under cyclic voltammetry conditions, scanning from 0 V to -1.5 V to +1.5 V to 0 V at 50 mV/s, in an electrochemical liquid cell filled with 0.6 mM $HAuCl_4$ **+** 0.1 M HCl (Supporting video 2). Liquid droplets (yellow arrows) are visible particularly after cycling to positive potentials.

This article is protected by copyright. All rights reserved.

Author Manuscript

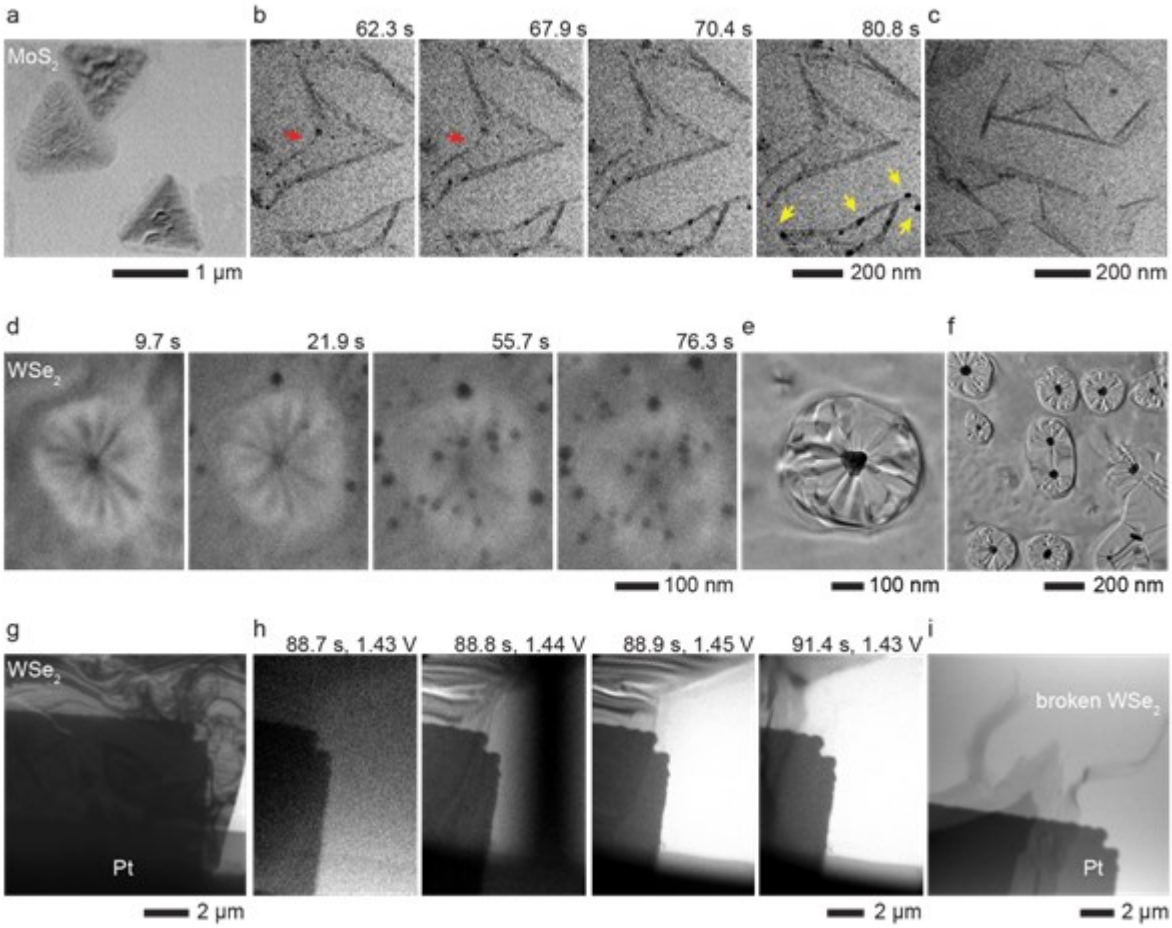

Figure 4: Mechanical and electrical stability of 2D materials. TEM images of as-grown MoS_2 flake (**a**) before flowing liquid and (**b**-**c**) after exposing to the electron beam and flowing 5 mM $HAuCl_4$. Red and yellow arrows indicate the dissolution and growth of Au nanoparticles respectively. (**d**) Time series of TEM images showing the formation of Au nanoparticles on WSe_2 inside a liquid cell filled with 5 mM $HAuCl_4$. (**e-f**) Post-growth TEM images showing representative Au nanoparticles on (or under) WSe_2. (**g-i**) TEM images of WSe_2 flake exfoliated onto a Pt electrode during CV scanning. (**g**) Before scanning; (**h**) rapid changes during scanning; (**i**) after scanning from 0 V to -1.5 V and back to 0 V at 50 mV/s in an electrochemical liquid cell filled with 0.6 mM $HAuCl_4$ **+** 0.1 M HCl.

This article is protected by copyright. All rights reserved.

Author Manuscript

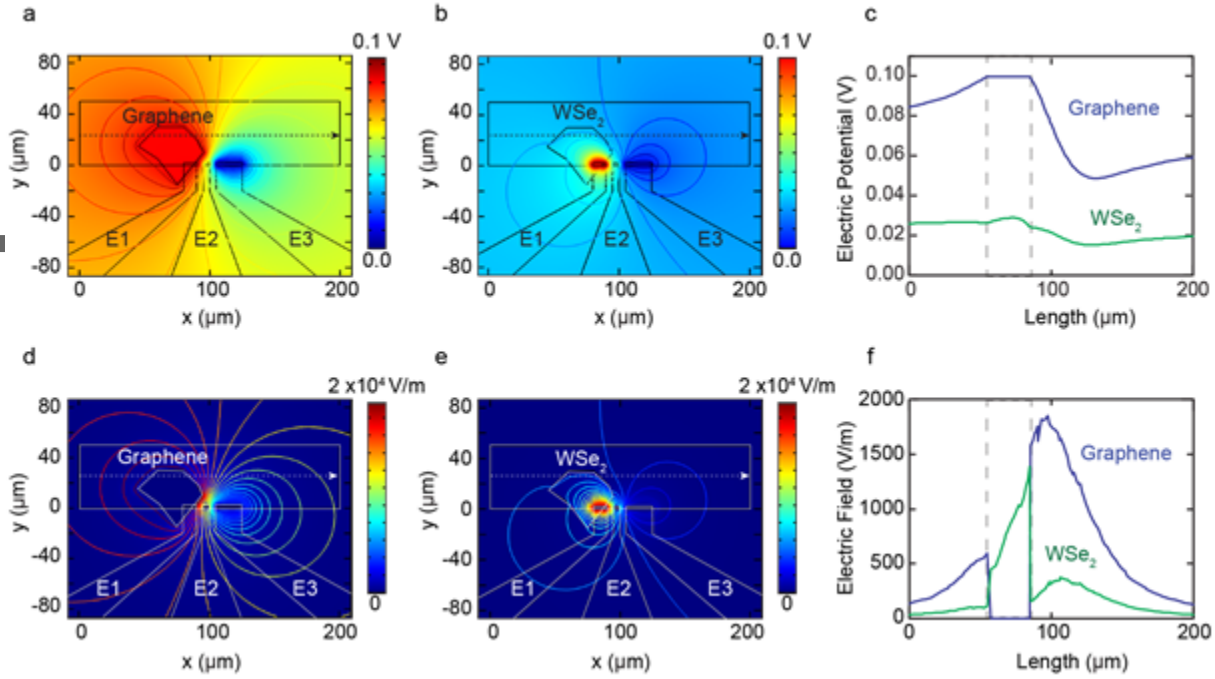

Figure 5: Numerical modelling of graphene *versus* WSe_2 electrodes. (**a**) Potential map (V) of Pt/graphene and (**b**) Pt/WSe_2 system where 0.1 V is applied to the working electrode (E1) with respect to the counter electrode (E3). The shape of the electrode used corresponds to an experimental exfoliated flake and the surrounding free area is assigned the properties of 0.1 M H_2SO_4 electrolyte. Contours are placed every 0.05 V and the arrow surface is proportional to current density. (**c**) 1D plot across the center of the SiN_x window (black dotted lines in panel a and b) of the electric potential change for graphene (blue) and WSe_2 (green) systems. (**d**) Electric field distribution (V/m) shown as a colour map for the Pt/graphene and (**e**) Pt/WSe_2 systems. Contours again represent electric potential (V) and are placed every 0.05 V. Electrochemical 'hotspots' can be observed at sharp corners of the 2D material flakes. (**f**) 1D plot across the center of the SiN_x window (white dotted lines in panel c and d) of the electric field change for graphene (blue) and WSe_2 (green) systems. The 2D flake positions are indicated as dotted grey lines in c and f.

$$Cu^{2+} + 2e^- \rightarrow Cu^0 \qquad \text{Equation 1}$$

$$Cu^0 \rightarrow Cu^{2+} + 2e^- \qquad \text{Equation 2}$$

$$d_m = \frac{mass\ thickness\ of\ the\ object}{mass\ thickness\ of\ the\ total\ liquid\ cell\ component} \qquad \text{Equation 3}$$

This article is protected by copyright. All rights reserved.

Author Manuscript

The electrode material used in liquid cell transmission electron microscopy plays an important role in determining both electrochemical performance and image resolution. We show, through experimental demonstration of metal deposition and modelling, that multilayer graphene acts as a suitable electrode for liquid cell electrochemical microscopy that enables interpretable and higher resolution quantitative electrochemical experiments.

Liquid Cell Electrochemistry

Shu Fen Tan, Kate Reidy, Serin Lee, Julian Klein, Nicholas M. Schneider, HaeYeon Lee and Frances M. Ross*

Multilayer Graphene – A Promising Electrode Material in Liquid Cell Electrochemistry

ToC figure

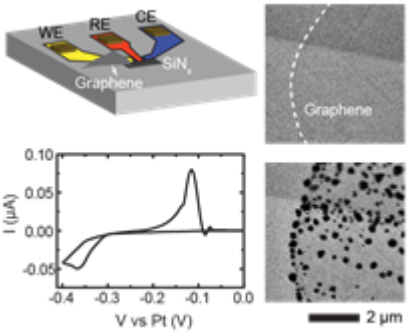

This article is protected by copyright. All rights reserved.